Acta Cryst. (1973). A**29**, 408

Optimally Spaced Rotational Grid Points*

BY DONALD E. WILLIAMS

Department of Chemistry, University of Louisville, Louisville, Kentucky 40208, *U.S.A.*

(*Received* 1 *December* 1972; *accepted* 8 *February* 1973)

Optimal rotational spacing was obtained for $n=2$ to 12 orientations of an object in three-dimensional space. For $n=2$, 3, and 4 the minimum spacing, χ(min), was 180°, with rotation space not being completely filled. For $n=5$ and 6 all spacings are equal to 151·05 and 141·06° respectively. The $n=7$ case has two spacings at 134·04 and 180°. The $n=8$ case has two spacings at 130·18 and 153·56°. The $n=10$ case has three spacings at 128·53, 141·05 and 164·8°. The $n=12$ case has two spacings at 120 and 180°. The best arrangement found for $n=9$ and 11 was to remove one grid point from $n=10$ and 12 respectively. The coordination about each point and the orientations of the grid difference rotation axes are given. The axes for $n=5$ are directed toward the vertices of a regular dodecahedron; the axes for $n=12$ are directed toward the vertices and faces of a cube. Products of two rotations of equal magnitude to give a third rotation of the same magnitude were considered and classified into conrotatory and disrotatory types. For $n>12$ the Lattman treatment was extended to include third-order terms. Examples of Lattmanian angle grids are given and the grid spacings are compared to theoretical estimates.

Introduction

Optimal rotational spacing as used here means an arrangement of n orientations of an object such that the magnitude of the least angle between orientations is maximum. The n orientations will be referred to as a rotational grid, and the angles between orientations will be referred to as intergrid angles. If some of the intergrid angles about a grid point are equal, they comprise a rotational coordination shell, in analogy with the usual concept of the distance coordination shell. The total number of rotational intergrid angles is $n(n-1)/2$; these can be thought of as filling the upper triangular part of a square matrix, excluding the diagonal elements.

Optimum rotational spacing, besides its purely mathematical interest, is of interest in connection with various practical rotational problems. If the initial orientation of an object is random, the choice of an optimally spaced rotational grid in rotation space will make it likely that at least one grid point is close to the starting orientation.

In the study of the structure of crystals containing rigid molecules a calculated Patterson function may be superposed for best fit onto the observed Patterson function, or some variation of this procedure may be used. Here the best orientation is unknown, and each optimized rotational-grid point provides a trial model to test or improve the fit. This subject has been discussed by Lattman (1972) and he gives references to recent work in this area.

* Supported by research grant GM16260 from the U.S. Public Health Service.

Minimization of the lattice energy of a crystal containing rigid molecules (molecular-packing analysis) is another example where optimal rotational spacing is of interest. The optimum rotational grid provides trial models on the energy surface such that at least one of them is likely to be sufficiently near the global minimum so as to avoid falling into a subsidiary or false minimum in the lattice energy. This subject has been discussed by Williams (1972) and he gives references to recent work in this area.

An alternative approach is to use the Monte-Carlo method (André, Fourme & Renaud, 1972) to generate trial rotational-grid points.

There are, of course, no rotations in one-dimensional space. In two-dimensional space the matrix representation of n optimally spaced rotational-grid points may be generated from the identity matrix by $(n-1)$ rotations through the angle $2\pi/n$. These contacts may be arranged into different spacings. For n even the most distant spacing is at 180° and has coordination number 1. There are $n/2-1$ nearer spacings each with coordination number 2. For n odd there are $(n-1)/2$ spacings, each of coordination number 2; no spacing occurs at 180°.

Product of two equal rotations in three dimensions

We consider here the matrix representation of the product of two successive rotations of equal angle, χ, about different axes. Let the first rotation be $\mathbf{R}_a(\chi,\mathbf{a})$ and the second be $\mathbf{R}_b(\chi,\mathbf{b})$, where the $\mathbf{R}_i$ are orthonormal matrices representing a counterclockwise rotation through angle χ about axis $\mathbf{i}$, a unit vector. In terms of the components of $\mathbf{a}$,

$$\mathbf{R}_a=\begin{bmatrix}\cos\chi+a_1^2(1-\cos\chi) & a_1a_2(1-\cos\chi)-a_3\sin\chi & a_1a_3(1-\cos\chi)+a_2\sin\chi\\ a_1a_2(1-\cos\chi)+a_3\sin\chi & \cos\chi+a_2^2(1-\cos\chi) & a_2a_3(1-\cos\chi)-a_1\sin\chi\\ a_1a_3(1-\cos\chi)-a_2\sin\chi & a_2a_3(1-\cos\chi)+a_1\sin\chi & \cos\chi+a_3^2(1-\cos\chi)\end{bmatrix}.$$

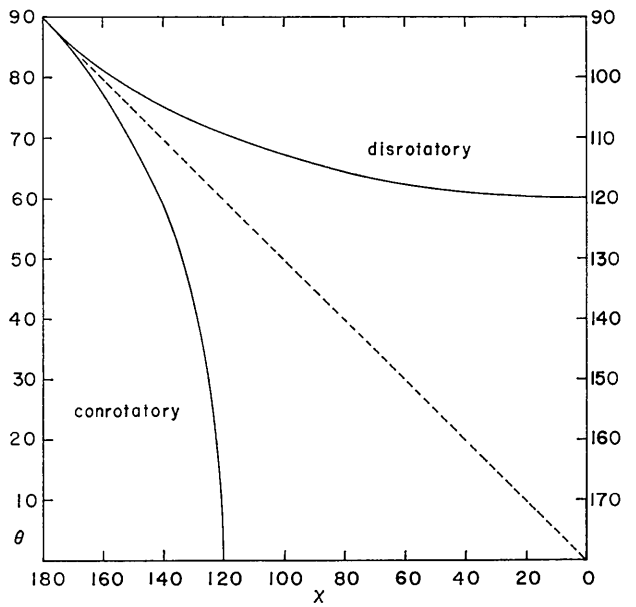

Fig. 1. Axial inclination, θ, *versus* rotation angle, χ, for the conrotatory and disrotatory combinations of three equal-angle rotations (°).

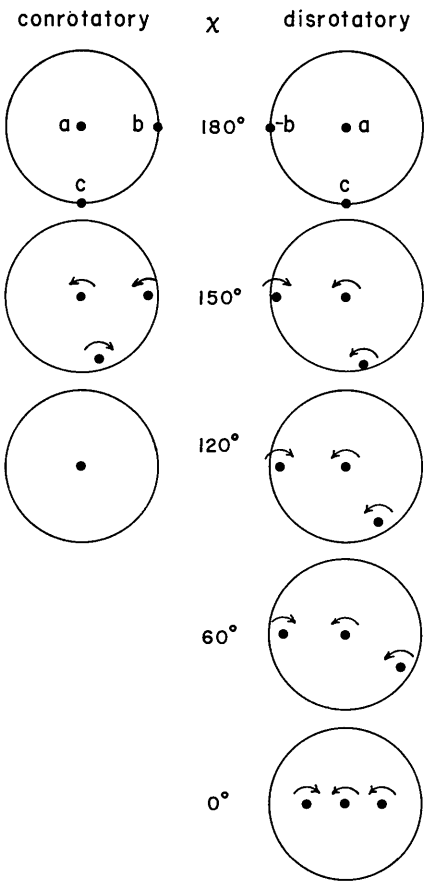

Fig. 2. The conrotatory and disrotatory axis directions are shown stereographically for several values of χ(°). The directions of rotation are indicated.

The rotational origin may be selected by taking **a** along the z axis and requiring **b** to lie in the xz plane. Let us further restrict ourselves to rotation products also having the amplitude $|\chi|$. This case is of interest in connection with equally spaced rotation grids. The product rotation, $\mathbf{R}_c$, is then equal to $\mathbf{R}_b\mathbf{R}_a$ and must have a trace equal to $1+2\cos|\chi|$. If tr $(\mathbf{R}_b\mathbf{R}_a)$ is expanded in components and set equal to tr $(\mathbf{R}_c)$, we obtain the equation

$$(1-\cos\chi)^2 b_3^2-(2\sin^2\chi)b_3-\sin^2\chi=0\,.$$

The solutions are

$$b_3=[\sin\chi/(1-\cos\chi)^2]\{\sin\chi\pm[2(1-\cos\chi)]^{1/2}\}\,.$$

The solutions depend on θ, the angle between vector **b** and the z axis, where, of course, $\cos\theta=b_3$. The direction of rotation of $\mathbf{R}_c$ has been lost but will be recovered later. Since we have chosen **b** in the xz plane $b_1=(1-b_3^2)^{1/2}$ and $b_2=0$. Fig. 1 gives a plot of the two solutions. For the disrotatory solution θ is in the range $90\leq\theta\leq180°$.

For purpose of drawing stereograms it is convenient to have the **b** axis in the upper hemisphere. Thus, if $\theta>90°$ we consider the reverse axis $-\mathbf{b}$ which has a clockwise rotation direction. The angle between $-\mathbf{b}$ and **z** is, of course, $180°-\theta$.

The direction of rotation for $\mathbf{R}_c$ may be recovered by evaluating its elements and comparing them to the elements of the product matrix $\mathbf{R}_b\mathbf{R}_a$. The solution we call conrotatory corresponds to the rotation directions $\mathbf{R}_c(-\chi,\mathbf{c})=\mathbf{R}_b(\chi,\mathbf{b})\mathbf{R}_a(\chi,\mathbf{z})$, where **b** is directed toward the upper hemisphere. The solution we will call disrotatory corresponds to the rotation directions $\mathbf{R}_c(\chi,\mathbf{c})=\mathbf{R}_b(-\chi,-\mathbf{b})\mathbf{R}_a(\chi,\mathbf{z})$, where $-\mathbf{b}$ is now directed toward the upper hemisphere. The axial directions are shown stereographically in Fig. 2.

The conrotatory case is easily understood by referring to Fig. 2. When $\theta=0°$ the solution is $\mathbf{R}_b=\mathbf{R}_a=\mathbf{R}(120°,\mathbf{z})$; obviously $\mathbf{R}_c=\mathbf{R}(-120°,\mathbf{z})$. As θ increases from zero the three axes separate symmetrically so that all interaxial angles are acute and equal to θ. For the inclined axes χ gradually increases from 120 to 180°; at $\chi=180°$, $\theta=90°$ and the axial symmetry is 222. No solution exists for the conrotatory case when $\chi<120°$.

The disrotatory case can be followed starting from $\chi=180°$. Here the two cases are equal since positive and negative rotations of 180° about the same axis are identical. Axis $-\mathbf{b}$ is shown in the stereograms. As χ decreases from 180°, $-\mathbf{b}$ moves upward toward the z axis in the xz plane. The product axis, **c**, moves into the $x\bar{y}z$ octant. The angles between **a** and $-\mathbf{b}$, and **a** and **c**, are acute and equal to $180°-\theta$. The angle between $-\mathbf{b}$ and **c** is obtuse and equal to θ. As χ decreases toward zero, θ approaches the limiting value of 120° and **c** approaches the xz plane inclined at 60° to **z**. This limit of $\mathbf{b}_3=-\frac{1}{2}$ as $\chi\to0$ can be verified by a series expansion of the equation for $\mathbf{b}_3$. When $\chi=0$ all three

axes are indeterminate, of course, since no rotations are involved.

Using these results, it will be possible in the following section to describe triads of equal-angle rotations in terms of conrotatory or disrotatory relationships.

Optimal spacing of n rotational-grid points in three dimensions

$n=2$, 3 *and* 4

For $n=4$ the rotation space is not completely filled. By this it is meant that additional orientational freedom exists after fixing the rotational origin. This is obviously true for $n=2$, since the direction of the single rotation axis relating the grid points is completely arbitrary. This direction is significant, however, for a general asymmetric object.

We will describe the solution for $n=4$; the $n=3$ solution may be obtained by deleting one orientation from $n=4$. Fig. 3 shows the optimum selection of the grid points. All intergrid angles are 180°. The first orientation is just the identity matrix, represented by the Cartesian axes $(x_1y_1z_1)$. The second orientation of axes, $(x_2y_2z_2)$, is obtained by a 180° rotation about the z axis. The third orientation, shown in the right side of the figure, is obtained by a 180° rotation about the x axis. The fourth orientation is then obtained from the third by a 180° rotation about the z axis again.

It is seen that all intergrid angles are indeed 180° so that the arrangement is optimum. Note, however, that the two axial orientations in the right side of the figure may be rotated an arbitrary amount about the z axis without changing any of the intergrid angles. This is the additional degree of freedom that was referred to above.

$n=5$

The four nonorigin rotation-grid points may be selected as rotations of $\chi=151{\cdot}05°$ ($\cos\chi=-\frac{7}{8}$) about tetrahedral axes. If the vertex numbering scheme shown in Fig. 4 is used, the matrices are $\mathbf{I}$, $\mathbf{R}_1$, $\mathbf{R}_3$, $\mathbf{R}_{12}$, and $\mathbf{R}_{14}$. The intergrid spacings are obtained by setting

$$\mathbf{D}_{jk}\mathbf{R}_j=\mathbf{R}_k\,,$$

or

$$\mathbf{D}_{jk}=\mathbf{R}_k\mathbf{R}_j^t\,.$$

The difference matrices, $\mathbf{D}_{jk}$, include the grid points themselves, since one of the $\mathbf{R}_j$ is the identity matrix. All of the difference matrices correspond to rotations of $\chi=151{\cdot}05°$ about axes directed toward the vertices of a regular dodecahedron. The dodecahedron, of course, includes the tetrahedron as a subfigure.

The vertex identification of the intergrid matrices is shown in Table 1. The Table is antisymmetric in the sense that the direction of rotation is reversed in the lower left portion of the table. Alternatively, the axial directions could be reversed, setting $\mathbf{R}_1^t=\mathbf{R}_{11}$, and so forth.

Table 1. *Axial identification of intergrid difference matrices,* $\mathbf{D}_{jk}$, *for* $n=5$

	$\mathbf{I}$	$\mathbf{R}_1$	$\mathbf{R}_3$	$\mathbf{R}_{12}$	$\mathbf{R}_{14}$
$\mathbf{I}$	$\mathbf{I}$	$\mathbf{R}_1$	$\mathbf{R}_3$	$\mathbf{R}_{12}$	$\mathbf{R}_{14}$
$\mathbf{R}_1$	$\mathbf{R}_1^t$	$\mathbf{I}$	$\mathbf{R}_9$	$\mathbf{R}_5$	$\mathbf{R}_7$
$\mathbf{R}_3$	$\mathbf{R}_3^t$	$\mathbf{R}_9^t$	$\mathbf{I}$	$\mathbf{R}_8$	$\mathbf{R}_{15}$
$\mathbf{R}_{12}$	$\mathbf{R}_{12}^t$	$\mathbf{R}_5^t$	$\mathbf{R}_8^t$	$\mathbf{I}$	$\mathbf{R}_{10}$
$\mathbf{R}_{14}$	$\mathbf{R}_{14}^t$	$\mathbf{R}_7$	$\mathbf{R}_{15}^t$	$\mathbf{R}_{10}^t$	$\mathbf{I}$

The products $\mathbf{R}_k=\mathbf{D}_{jk}\mathbf{R}_j$ are all conrotatory as designated in the previous section. In Fig. 2 the axis of $\mathbf{R}_j$ corresponds to **a**, the axis of $\mathbf{D}_{jk}$ corresponds to **b**, and the axis of $\mathbf{R}_k$ corresponds to $-\mathbf{c}$. For $\chi=151{\cdot}05°$ axes **a** and **b** subtend an angle of 70·5°, **a** and $-\mathbf{c}$ subtend an angle of 109·5°, and **b** and $-\mathbf{c}$ subtend an angle of 109·5° also. Thus it can be seen from Fig. 4 how Table 2 is made up from conrotatory product rotations. There is no mixing of rotation directions, and there is an enantiomorphous set of grid points with reversed rotation directions.

$n=6$

A computer program was written to find the optimum orientation of n rotational grid points. This program found the minimum of the function

$$F=\sum|\chi_{jk}|^{-r}$$

where χ_{jk} was found from the difference matrices, $\mathbf{D}_{jk}$, which in turn were found from the set of n matrices

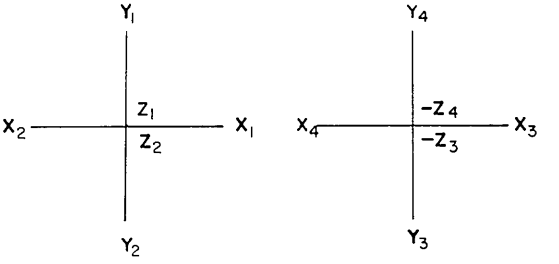

Fig. 3. An orientation of four Cartesian-coordinate systems such that all rotation angles are 180°.

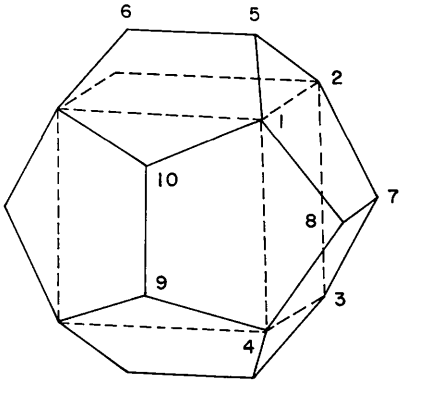

Fig. 4. A numbering system for the vertices of a regular dodecahedron. Add 10 to get the vertex number of the vertices related by the center of symmetry.

I, $\mathbf{R}_i$, $i=1,2,\ldots,(n-1)$. The starting model was the optimum grid in two dimensions. The exponent, r, was initially set at 12 and then increased to a large value, at least 200, as the refinement progressed. As r becomes large, minimization of F is equivalent to maximizing the least intergrid angle.

Each matrix $\mathbf{R}_i$ is orthonormal and is specified by three parameters, so that the minimization problem involved $3(n-1)$ variables. A grid-search technique in the parameter space was used to locate the minimum. In general, smooth convergence was obtained to the results reported here; an exception was the case of $n=9$, where a false minimum was encountered (see below).

For $n=6$ it was found possible to make all intergrid angles equal, with $|\chi|=141{\cdot}06°$. The axial arrangement is shown in Fig. 5. The symmetry of the axes of the difference matrices is $4/mmm$. Both conrotatory and disrotatory products are utilized; the figure indicates the intergrid axes by type (C or D), as well as the generating grid points.

One grid axis may be taken along **z**, and the other four have fourfold symmetry about **z**, inclined at 60° to the z axis. A mirror-related difference axis appears such that, for example, the projected angle onto the xy plane of grid axis 2 and conrotatory difference axis $C46$ is 19·5°. Thus, the projected angle between grid axis 2 and difference axis $C36$ is tetrahedral. The other four difference axes are disrotatory and also show fourfold symmetry about **z**; they are inclined at 45° to the z axis. The overall difference-axis orientation pattern may be described as a set of Cartesian axes and sets of axis triplets oriented about the [111] directions.

$n=7$

This case presents the first appearance of different rotational spacings in three dimensions. Of the 21 intergrid angles, 18 are at 134·04° and 3 are at 180°. Fig. 6 shows the location of the grid and difference axes. The symmetry of the axes is 222.

There are two types of grid axes: $\mathbf{R}_2$, $\mathbf{R}_3$, and $\mathbf{R}_4$ are in the xy, yz, and xz planes, subtending an angle of

Table 2. *Rotation angles and axial directions for optimally spaced rotational grids in three dimensions*

The first grid point is always taken as an identity matrix. $x=0{\cdot}57735$.

n	χ(°)	a_1	a_2	a_3	θ_+	θ_2	θ_-
5	151·05	x	x	x	228·18	104·48	90·00
	151·05	x	$-x$	$-x$	131·82	104·48	270·00
	151·05	$-x$	$-x$	x	588·18	104·48	90·00
	151·05	$-x$	x	$-x$	491·82	104·48	270·00
6	141·06	0·85355	−0·14645	0·50000	610·53	109·47	340·53
	141·06	−0·85355	0·14645	0·50000	250·53	109·47	340·53
	141·06	0·14645	0·85355	0·50000	250·53	109·47	160·53
	141·06	−0·14645	0·85355	0·50000	250·53	109·47	199·47
	141·06	0·0	0·0	−1·0	—	180·00	218·94
7	134·04	0·95590	0·29371	0·0	360·00	134·04	34·16
	134·04	0·0	0·95590	0·29371	290·59	123·29	180·00
	134·04	0·29371	0·0	0·95590	227·85	211·37	0·0
	134·04	−0·42407	−0·80021	0·42407	630·00	112·97	124·16
	134·04	0·42407	−0·42407	−0·80021	124·16	247·03	270·00
	134·04	−0·80021	0·42407	−0·42407	450·00	112·97	304·16
8	153·56	0·95050	0·31073	0·0	360·00	153·56	36·21
	153·56	0·0	−0·95050	−0·31073	105·82	135·43	180·00
	153·56	−0·31073	0·0	0·95050	567·77	215·21	0·0
	130·18	x	$-x$	x	617·62	95·55	270·00
	130·18	−0·80690	x	0·12483	329·91	128·28	288·83
	130·18	$-x$	−0·12483	−0·80690	120·16	244·79	24·40
	130·18	0·12483	0·80690	$-x$	462·38	95·55	162·41
10	141·05	0·0	−0·70711	−0·70711	126·86	263·62	180·00
	141·05	−0·70711	0·0	0·70711	593·14	263·62	0·0
	141·05	0·70711	0·70711	0·0	360·00	141·05	90·00
	128·53	0·90449	−0·42226	−0·05990	14·17	128·11	309·95
	128·53	−0·42226	0·90449	0·05990	345·83	128·11	230·05
	128·53	0·42226	0·05990	0·90449	236·11	225·19	16·15
	128·53	−0·90449	−0·05990	−0·42226	82·44	109·48	7·58
	128·53	−0·05990	−0·90449	0·42226	637·56	109·48	172·42
	128·53	0·05990	0·42226	−0·90449	483·89	225·19	163·85
12	180·00	1·0	0·0	0·0	—	180·00	0·0
	180·00	0·0	1·0	0·0	—	180·00	180·00
	180·00	0·0	0·0	1·0	180·00	0·0	—
	120·00	x	x	x	270·00	90·00	90·00
	120·00	$-x$	$-x$	$-x$	90·00	90·00	90·00
	120·00	$-x$	x	x	270·00	90·00	270·00
	120·00	x	$-x$	$-x$	90·00	90·00	270·00
	120·00	$-x$	$-x$	x	630·00	90·00	90·00
	120·00	x	x	$-x$	450·00	90·00	90·00
	120·00	x	$-x$	x	630·00	90·00	270·00
	120·00	$-x$	x	$-x$	450·00	90·00	270·00

17·08° with the x, y, and z axes respectively. Difference matrices formed from disrotatory products $\mathbf{D}_{34}$, $\mathbf{D}_{24}$, and $\mathbf{D}_{23}$ are located symmetrically about the Cartesian axes.

Grid matrices $\mathbf{R}_5$, $\mathbf{R}_6$, and $\mathbf{R}_7$ are parts of square arrays centered on the Cartesian axes such that the projected angle is 36·85°. The other vertices of the squares are formed by difference axes resulting from conrotatory products involving two different types of grid axes. The three remaining axes are in the Cartesian directions. They correspond to the difference matrices within the set $\mathbf{R}_5$, $\mathbf{R}_6$, and $\mathbf{R}_7$. These difference-matrix axes are called mixed since the rotation angles are different.

$n=8$

The 28 intergrid contacts are separated into two spacings. The first spacing has 22 contacts at 130·18°; the second spacing has six contacts at 153·56°. Fig. 7 shows the grid points and the intergrid axes. The first spacing has an interpenetrating block-type arrangement, with additional line figures across the axes. The second spacing has three additional line figures formed by rotating the first spacing-line figures by 90°. Both conrotatory and disrotatory equal-product rotations are used as indicated in the Figure, as well as the mixed-product rotations. The symmetry of the axes is 222.

$n=10$ (*and* $n=9$)

For $n=10$ the 45 contacts are arranged in three spacings. The first spacing has 36 contacts at 128·53°; the second spacing has 6 contacts at 141·05°; and the last spacing has three contacts at 164·8°. The grid points and intergrid-axis orientations are shown in Fig. 8. The triply degenerate spacing at 164·8° has axes which are coincident with the Cartesian axes. The three pairs of axes in the spacing at 141·05° are arranged to bisect each pair of Cartesian axes.

The nearest-neighbor contacts are arranged in four triplets centered about the [111] directions, and six quartets symmetrically disposed about the xy, xz, and yz planes. The intergrid axial symmetry is 432. Note that points -5 and 6 are below and above the xy plane, and the similarly disposed M axes are out of the xy plane.

The triplets result from equal-product conrotatory or disrotatory axis combinations are indicated in the Figure. The six quartets arise from mixed-product rotations.

The computer calculation for $n=9$ obtained a false minimum with a smaller χ(min) than that obtained for $n=10$.

The best solution found for $n=9$ was simply to remove one grid point from the $n=10$ case.

$n=12$ (*and* $n=11$)

The case of $n=12$ is especially straightforward. The 66 intergrid contacts are arranged in two spacings. The nearest-neighbor spacing has 48 contacts at 120°; the second spacing has 18 contacts at 180°. The 120° grid axes, as well as all of the 120° intergrid axes, are arranged in the eight [111] directions. The three 180° grid axes, as well as all of the 180° intergrid axes, are in the three Cartesian directions. The difference matrices

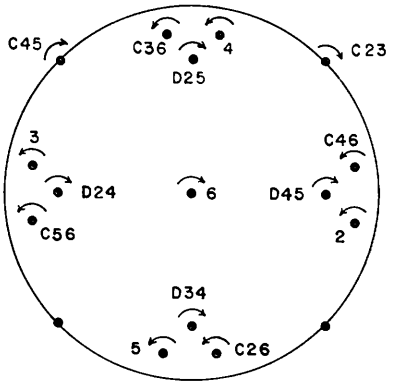

Fig. 5. Axial stereogram for $n=6$. In Figs. 5–8 the letters, C, D, and M indicate conrotatory, disrotatory, or mixed-type difference axes respectively. A negative sign means the grid axis is directed downward.

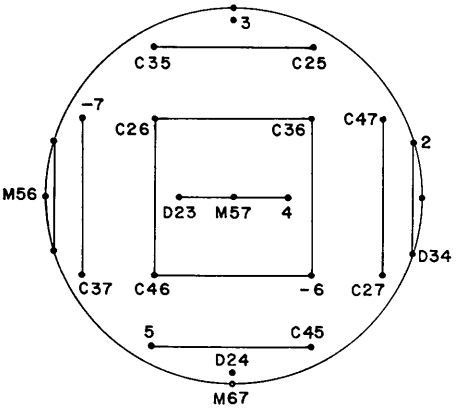

Fig. 6. Axial stereogram for $n=7$.

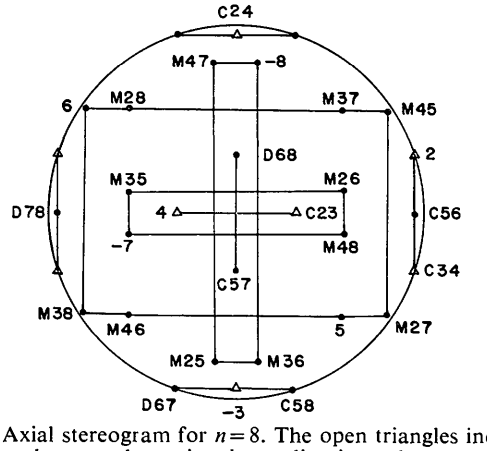

Fig. 7. Axial stereogram for $n=8$. The open triangles indicate the second rotational coordination sphere.

are formed from conrotatory products, with both directions of rotation being present simultaneously.

The best solution found for the $n=11$ case was simply to remove one point from the $n=12$ case.

Table 2 lists for reference the optimum grid data for $n=5$, 6, 7, 8, 10, and 12.

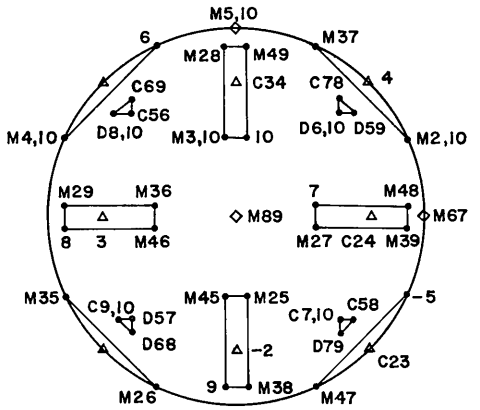

Fig. 8. Axial stereogram for $n=10$. The open triangles and squares indicate the second and third rotational coordination spheres.

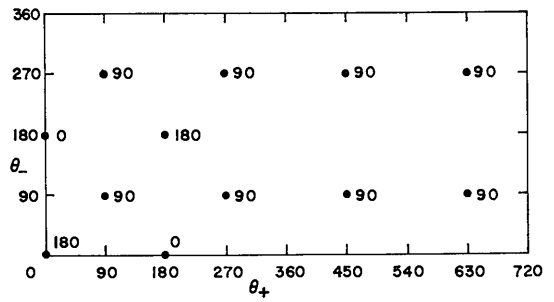

Fig. 9. Lattmanian angle plot of the optimum rotation grid for $n=12$. Elevations in θ_2 are given beside each point.

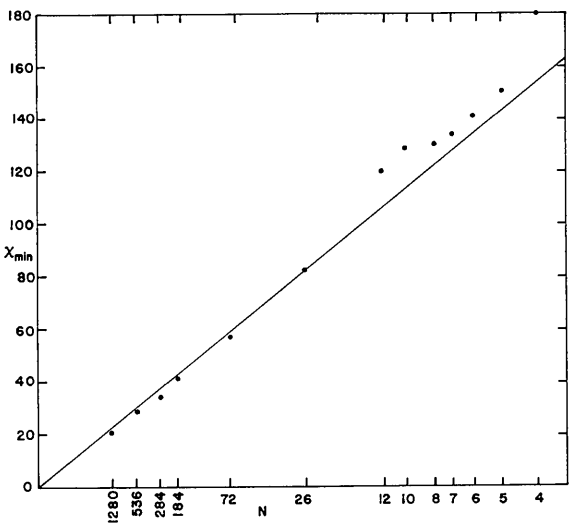

Fig. 10. The minimum intergrid angle, χ(min), as a function of $n^{-1/3}$. The solid line represents the values $\chi(\min)=245{\cdot}80\ n^{-1/3}$. The points for $n\leq 12$ are optimum: the points for larger n are taken from Table 4.

Coordination shells for $n\leq 12$

The rotational contacts about a given grid point may be characterized into coordination shells. Since rotation space is closed (as contrasted with translation space), the maximum possible intergrid angle is 180°. Table 3 lists the rotational coordination shells for the optimum grid systems with $n\leq 12$. The points are arranged into equivalent coordination types (no more than two types are needed in this range of n), with multiplicity $g_\alpha(\alpha=a,b)$. Each coordination type has coordination shells (no more than two shells are needed for this range of n) with individual multiplicities $h_{\alpha i}(i=1,2)$.

Table 3. *Coordination-shell data for optimum rotational grid points,* $n\leq 12$ *(angles in degrees)*

			First shell		Second shell	
n	α	g_α	$h_{\alpha 1}$	$\|\chi\|$	$h_{\alpha 2}$	$\|\chi\|$
2	*a*	2	1	180		
3	*a*	3	2	180		
4	*a*	4	3	180		
5	*a*	5	4	151·05		
6	*a*	6	5	141·06		
7	*a*	4	4	134·04		
	b	3	4	134·04	2	180
8	*a*	4	7	130·18		
	b	4	4	130·18	3	153·56
10	*a*	6	8	128·53	1	164·86
	b	4	6	128·53	3	141·05
12	*a*	12	8	120	3	180

An example of the interpretation of Table 3 is as follows. For $n=10$ there are 4 grid points of type *b*. Each of these points is surrounded by a coordination sphere of 6 points at 128·53° and another coordination sphere of 3 points at 141·05°.

Lattmanian angle grids

The case of large n has been treated recently by Lattman (1972). The optimum arrangement of the rotational-grid points may be described by Lattman's angles, θ_+, θ_2, and θ_-, which are defined in terms of the usual Eulerian angles θ_1, θ_2, and θ_3:

$$\begin{aligned} \theta_+ &= \theta_1+\theta_3 & 0\leq\theta_+<4\pi \\ \theta_2 &= \theta_2 & 0\leq\theta_2\leq\pi \\ \theta_- &= \theta_1-\theta_3 & 0\leq\theta_-<2\pi\,. \end{aligned}$$

The ranges of the Lattmanian angles are shown, except that when $\theta_2=0$ the range for θ_+ is reduced to $0\leq\theta_+<2\pi$. Optimum sampling of rotation space is obtained by taking equal intervals in $\Delta\theta_+\cos(\theta_2/2)$, $\Delta\theta_2$, and $\Delta\theta_-\sin(\theta_2/2)$.

We have verified Lattman's treatment and have extended the series expansion to include fourth-order terms. While the fourth-order terms enter the difference angle expression in a complicated way, the third-order terms are quite simple and may easily be included to yield the following third-order approximation:

$$\chi_d^2=\Delta\theta_+^2\cos^2(\theta_2/2)+\Delta\theta_2^2+\Delta\theta_-^2\sin^2(\theta_2/2) +(\Delta\theta_2/2)\cos(\theta_2/2)\sin(\theta_2/2)(\Delta\theta_-^2-\Delta\theta_+^2)\,.$$

Table 4. *Sample data for Lattmanian grids with* 3, 4, 5, 6, 7 *and* 9 *sections in* θ_2 (°)

Number of points	Theoretical χ(min)	Observed χ(min)	Number of sections	Section number	θ_2	$\Delta\theta_+$	$\Delta\theta_-$
26	82·97	82·82	3	1	0	90	–
				2	90	120	120
				3	180	–	90
72	59·08	57·91	4	1	0	60	–
				2	60	72	120
				3	120	120	72
				4	180	–	60
184	43·22	41·53	5	1	0	45	–
				2	45	45	120
				3	90	60	60
				4	135	120	45
				5	180	–	45
284	37·89	34·22	6	1	0	36	–
				2	36	36	120
				3	72	45	60
				4	108	60	45
				5	144	120	36
				6	180	–	36
536	30·26	28·97	7	1	0	30	–
				2	30	30	120
				3	60	36	60
				4	90	45	45
				5	120	60	36
				6	150	120	30
				7	180	–	30
1280	22·78	20·78	9	1	0	22·5	–
				2	22·5	22·5	120
				3	45	22·5	60
				4	67·5	30	45
				5	90	30	30
				6	112·5	45	30
				7	135	60	22·5
				8	157·5	120	22·5
				9	180	–	22·5

Thus, the third-order terms vanish when $\Delta\theta_+ = \Delta\theta_-$, as would be the optimum case when $\theta_2 = 90°$. When $\theta_2 \neq 90°$, generally the optimum $\Delta\theta_+$ would be different from the optimum $\Delta\theta_-$ and the third-order terms would require taking the equal intervals,

$$\Delta\theta_+\{\cos(\theta_2/2)[\cos(\theta_2/2) - (\Delta\theta_2/2)\sin(\theta_2/2)]\}^{1/2}$$

and

$$\Delta\theta_-\{\sin(\theta_2/2)[\sin(\theta_2/2) + (\Delta\theta_2/2)\cos(\theta_2/2)]\}^{1/2}.$$

Examples of Lattmanian angle grids

Fig. 9 shows the case of $n = 12$ plotted as a function of the Lattmanian angles. There are three sections in θ_2, with $\Delta\theta_2 = 90°$. Eight grid points are on the section $\theta_2 = 90°$ with $\Delta\theta_+ = \Delta\theta_- = 180°$. These points are staggered with respect to the pairs of points at $\theta_2 = 0°$ and $\theta_2 = 180°$. Note that at $\theta_2 = 0°$, θ_- is indeterminate, and at $\theta_2 = 180°$, θ_+ is indeterminate.

Sample data for Lattmanian angle grids with 3, 4, 5, 6, 7, and 9 sections in θ_2 are given in Table 4. No staggering of the sections was attempted, but the closest-to-optimum spacing of integral numbers of grid points was selected for each section. All intergrid angles were found and the closest contacts were determined. The degree of optimization may be estimated by comparing this minimum angle with a theoretical value obtained by dividing the total volume of Lattmanian angle space into n cubes of volume $\chi(\text{min})^3$. Thus, to the second-order approximation,

$$n\chi(\text{min})^3 = \int_0^{4\pi}\int_0^{\pi}\int_0^{2\pi} \cos(\theta_2/2)\sin(\theta_2/2)\,d\theta_-\,d\theta_2\,d\theta_+ = 8\pi^2$$

or $\chi(\text{min}) = 245{\cdot}80\ n^{-(1/3)}$ in degrees. Note that this theoretical value is not optimum, even for large n, since no staggering of the points is considered (compare hexagonal closest packing or face-centered cubic closest packing of points in translation space). However, this procedure is analogous to the frequently used simple-cubic grids in translation space.

Table 4 shows that the sample grids approach fairly closely these theoretical values for χ(min). Fig. 10 shows a plot of χ(min) *versus* $n^{-(1/3)}$ for all grids considered in this paper. The optimized values in the range $4 \leq n \leq 12$ are always better than the above theoretical estimate. For $n > 12$ the values for χ(min) are reasonably close to, but always less than, these theoretical values.

References

André, D., Fourme, R. & Renaud, M. (1972). *Acta Cryst.* A**28**, 458–463.
Lattman, E. A. (1972). *Acta Cryst.* B**28**, 1065–1068.
Williams, D. E. (1972). *Acta Cryst.* A**28**, 629–635.